OBJECT TRACKING EXTENSIONS FOR ACCURATE RECOVERY OF RAINFALL MAPS USING MICROWAVE SENSOR NETWORK

Yoav Liberman

Tel Aviv University
School of Electrical-Engineering
Tel Aviv, Israel

ABSTRACT

Recently, diverse methods have been proposed for faithful reconstruction of instantaneous rainfall maps by using received signal level (RSL) measurements from commercial microwave network (CMN), especially in dense networks. The main lacking of these methods is that the temporal properties of the rain field had not been considered, hence their accuracy might be limited. This paper presents a novel method for accurate spatio-temporal reconstruction of rainfall maps, derived from CMN, by using an extension to object tracking algorithms. An efficient coherency algorithm is used, which relates between sequential instantaneous rainfall maps. Then by using Kalman filter, the observed rain maps are predicted and corrected. When comparing the estimates to actual rain measurements, the performance improvement of the rainfall mapping is manifested, even when dealing with a rather sparse network, and low temporal resolution of the measurements. The method proposed here is not restricted to the application of accurate rainfall mapping.

Index Terms— Microwave Network, Object Tracking, Estimation, Reconstruction, Rainfall Mapping.

1. INTRODUCTION

The use of RSL measurements from CMN, for rainfall monitoring and mapping, was proven to be beneficial for numerous applications [1]. The well-known relation between the attenuation $A(dB/km)$ of a microwave signal strength and rainfall $R \ (mm/h)$, which is the main source for the signal's power degradation, is given by:

$$A = \alpha R^{\beta} \tag{1}$$

where the parameters α and β are, in general, functions of link frequency, polarization, and drop size distribution [2].

An example of a typical attenuation during a rain event is shown in Fig. 1. In the figure, the attenuation was measured on 18-January-2010, with 15 minutes time intervals and 0.1 dB of magnitude resolution, for a single 14 km link, operating at a frequency of 19.8 GHz, in the center-south of Israel. In the same figure, a rather sparse distribution of 36 available wireless microwave links (ML) in space, denoted as

black lines, is also shown. Where each link operate in typical frequency of 18-23 GHz, and length of 1-20 km. Most of the RSL measurements are available in a temporal resolution of 15 minutes, with 0.1 dB of magnitude resolution.
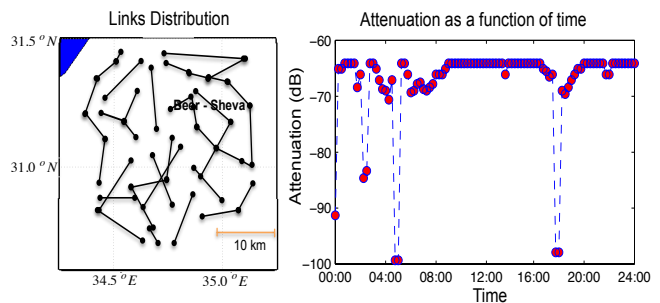

Fig. 1. Right: Example of 24 hours of measured attenuation (dB) as a function of time. Left: The operating ML over an area of $35X35 \ km^2$, provided by Cellcom ltd.

In the last decade some methods had been proposed for using RSL measurements from commercial wireless ML for the purpose of rainfall monitoring and mapping (e.g., [3, 4] etc.). The main shortcoming of these methods is that non of them had used the temporal properties of the rain field, hence, their accuracy is not only limited but also heavily dependent on the density of the CMN.

In 2009 Zinevich et al. offered to solve the differential advection equation in order to reconstruct the rain field dynamics, mainly for the purpose of achieving a larger coverage of the reconstruction, as detailed in [5]. The main lacking of this approach is that the RSL measurements must be available in a very high temporal resolution (e.g., 1 minute), and the deployed network is restricted to be rather dense, which is not always possible. Moreover, due to the complexity and non linearity of the differential equation, a numerical solution must be used. Hence, the solution may be numerically unstable, non unique and singular, as detailed in [6].

For the analysis in this paper, the method proposed by Liberman et al. in [7] for optimal recovery of instantaneous rain fall maps, given measurements from CMN, was adopted. Liberman et al. offered a technique which ensures an optimal and unique recovery of instantaneous rainfall maps, if some regularity conditions (mainly regarding the links distribution

in space) are satisfied. Moreover, in their work the authors managed to prove that the proposed method is very accurate, especially in a dense network. It should be noted that any instantaneous rainfall mapping technique may be used for the proposed application of accurate recovery of rainfall maps.

This paper presents a novel algorithm for accurate recovery of rainfall maps and their dynamics given RSL measurements. An approach, which constructs some model that relates between sequential rainfall maps is offered, the method uses an extension to the Coherency Sensitive Hashing (CSH) algorithm. The CSH efficiently finds matching patches between sequential frames. The method relies on hashing (similar patches are mapped to the same bin) and on image coherence, in order to propagate good matches between sequential frames. The decision on similar patches is obtained by defining some distant measure between candidate patches. The CSH is fully detailed in the work done by Korman et al. [8].

Afterwards, the Kalman filter for object tracking is used [9], which allows to optimally predict and correct the observed rainfall estimates. Therefore, it is not only possible to achieve higher spatial resolution, but also very high accuracy of the reconstruction, even when the temporal resolution of the measurements is rather low (15 minutes), and the provided network is rather sparse.

By inspecting a significant rain event in the center south of Israel, it is shown that the proposed method outperforms the other rainfall mapping techniques (e.g., Radar, Zinevich et al. method and the instantaneous mapping), almost uniformly, when compared to actual rain measures in given locations.

This paper is organized as follows: Section 2 details the method for spatio-temporal reconstruction of rainfall maps, given RSL measurements from CMN . In Section 3 real data results and performance evaluation of the proposed method are demonstrated. This paper is discussed in Section 4.

2. THE SPATIO-TEMPORAL RECONSTRUCTION

The basic assumption of a space-time model for rainfall mapping is that the distribution of the rain intensity, in each inspected location, might be considered as a conserved quantity over an intermediate time intervals (e.g., 15-30 minutes) [5]. While in [5] the rain field was assumed to slightly differ between sequential instantaneous rainfall maps, here this assumption is not valid, due to the longer time intervals. Hence, a different approach for the spatio-temporal reconstruction of rainfall maps is vital.

For the discussion here, I_t and I_{t+1} are regarded as the two sequential instantaneous rainfall maps. In the sequel, a model that relates between points of interest in I_t to their matching points in I_{t+1} is constructed, so that the following, general, linear relation is satisfied:

$$\begin{bmatrix} x_{i;t+1} \\ y_{i;t+1} \end{bmatrix} = \begin{bmatrix} a & b & c \\ d & e & f \end{bmatrix} \begin{bmatrix} x_{i;t} \\ y_{i;t} \\ 1 \end{bmatrix} = \mathbf{H} \begin{bmatrix} x_{i;t} \\ y_{i;t} \\ 1 \end{bmatrix} \quad (2)$$

Where $[x_{i;t}, y_{i;t}]^T$ indicates the coordinate of the i_{th} point of interest in space, for each time step t. The unknown parameters a, b, d, e stand for the rotation and scale factors, and c, f are the translation factors. It should be noted that $\mathbf{H}$ in (2) is sometimes regarded as a 2D affine relation matrix.

Though a linear relation might be limited, it was not only shown in [7] that by correctly choosing $\mathbf{H}$, (2) is in most cases accurate, but also, linear relations are vastly used in meteorological and hydrological applications (e.g., [10]) for modelling precipitation propagation. Hence, it is plausible to assume that kind of relation. Because our goal is to form an accurate model which relates between each $[x_{i;t+1}, y_{i;t+1}]^T$ to its corresponding coordinate $[x_{i;t}, y_{i;t}]^T$, by denoting $\vec{\theta} \triangleq [a, b, c, d, e, f]^T$, (2) may be rewritten as:

$$\begin{bmatrix} x_{i;t+1} \\ y_{i;t+1} \end{bmatrix} = \begin{bmatrix} ax_{i;t} + by_{i;t} + c \\ dx_{i;t} + ey_{i;t} + f \end{bmatrix} \quad (3)$$

Now, by reforming (3), the following relation in terms of $\vec{\theta}$ might be derived, that is:

$$\begin{bmatrix} x_{i;t} & y_{i;t} & 1 & 0 & 0 & 0 \\ 0 & 0 & 0 & x_{i;t} & y_{i;t} & 1 \end{bmatrix} \vec{\theta} =$$
$$= \mathbf{B}(x_{i;t}, y_{i,t}) \vec{\theta} = \begin{bmatrix} x_{i;t+1} \\ y_{i;t+1} \end{bmatrix} \quad (4)$$

hence, for N corresponding matching points, $i = 1, 2 \ldots N$. One can see that the relation matrix can be formed from (4) by estimating $\vec{\theta}$ as the least squares (LS) solution. This is of course possible if and only if there are at least 3 matching points between the inspected sequential frames at time t and $t + 1$, that is, there are at least 3 points of interest in I_t that correspond to their matching points in I_{t+1}. Thus, by denoting: $\tilde{\mathbf{B}} = [\mathbf{B}^T(x_{1;t}, y_{1,t}) \ldots \mathbf{B}^T(x_{N;t}, y_{N,t})]^T$ and $\vec{x}_{t+1} = [x_{1;t+1}, y_{1;t+1} \ldots x_{N;t+1} \ y_{N;t+1}]^T$, the LS solution may be obtained as follows:

$$\hat{\theta} = (\tilde{\mathbf{B}}^T \tilde{\mathbf{B}})^{-1} \tilde{\mathbf{B}}^T \vec{x}_{t+1} \quad (5)$$

where $\hat{\theta}$ is the estimated $\vec{\theta}$, with $dim(\vec{\theta}) = 6X1, dim(\tilde{\mathbf{B}}) = 2NX6, dim(\vec{x}_{t+1}) = 2NX1$.

In order to establish the desired relation matrix $\mathbf{H}$, an extension to the Coherency Sensitive Hashing (as described in Section 1) method is proposed, so the required matching points could be obtained. Therefore, an iterative algorithm is proposed in order to extract the desired points in some predefined area of interest, given two instantaneous sequential rainfall maps, denoted as I_t and I_{t+1}. The novel algorithm is detailed in **Algorithm 1**.

The proposed algorithm performs well, as can be observed in Fig. 2, which shows the derived matching points between two instantaneous sequential reconstructions of the rain field, for a rain cloud system moving from south-west towards north-east. The black lines in the figures indicate the 36 available operating links in the area of interest, which is

about $35X35\ km^2$. The blue arrows indicate the direction of the rain field dynamics in space, provided the detected points of interest in I_t and their matching points in I_{t+1}.

Algorithm 1 Points Of Interest Detection

1: Set $iter = 0$ (iteration number) and set the Rain Intensity Search (RIS_0) to include only the dominant rain intensities observed in I_t, that is $RIS_0 = [Max(I_t) - \epsilon,\ Max(I_t)]$. Where ϵ is small enough with respect to $Max(I_t)$, e.g., $\epsilon = Max(I_t)/10$. $dim(RIS_{iter}) = 2$.
2: Find the N coordinates of interest in I_t: $[x_{i;t}, y_{i;t}]$ for $i = 1, 2...N$, which correspond to the current RIS_{iter} within the area of interest.
3: Use the efficient CSH algorithm between I_t and I_{t+1}, in order to find the matching coordinates in I_{t+1}, which correspond to the coordinates of interest in I_t.
4: Sort all matching points with respect to the direction in which they were found (e.g., Eastern, Western etc.).
5: Form an histogram of all the matching points direction in degrees (e.g., 45° - North East, 90° - North; etc.).
6: If a prior information is available, define a plausible range (e.g., toward East - 0° to 90°) for the **Main Direction**, which indicates the possible rain dynamics movement.
7: Include all the matching points which correspond to the range of direction angles around the direction that received the highest probability observed in step (5), which is the **Main Direction**. The included points are the "Chosen Directions", do not consider any matching points which are not contained within the "Chosen Directions".
8: **if** $N < 3$ or the **Main Direction** is not inside the range defined in step (6) (e.g., for only Eastern directions, the **Main Direction** may vary between 0° to 90°); **then**
9: $iter = iter + 1$.
   $RIS_{iter} = [RIS_{iter-1}[0] - \epsilon,\ Max(I_t)]$.
10: **if** $RIS_{iter}[0] \approx 0$; **then**
11: No Matching points were detected
12: **return**
13: **else**
14: Go to step (2).
15: **end if**
16: **else**
17: Save the obtained matching points from step (7).
18: **return** .
19: **end if**

The histogram in Fig. 2 is the histogram for the directions obtained from all the points of interest in I_t (i.e., step (3) in **Algorithm 1**), which accounts for a total of 189 points.

As mentioned before, due to a prior information regarding the rain field movement towards east, the range for the **main direction** from step (6) was assumed to vary from 0° to 90°. According to step (7) in **Algorithm 1**, 169 points of interest were considered in the analysis ($N \gg 3$), these correspond to the surrounding of the **Main Direction**, which observed the

highest probability ($\sim 65^o$). From Fig. 2, one can see that a small cloud ($30.05^o N,\ 34.4^o E$) was also present in I_{t+1}. If not for step (7), false directions would have been obtained, so errors would surely be observed in the dynamical recovery.

The example shown in Fig. 2 was obtained from the 18-Jan-2010 rain event occurred in the south-center of Israel, for RSL data received from 36 operating ML. The ML distribution in the area of interest is considered to be rather sparse.
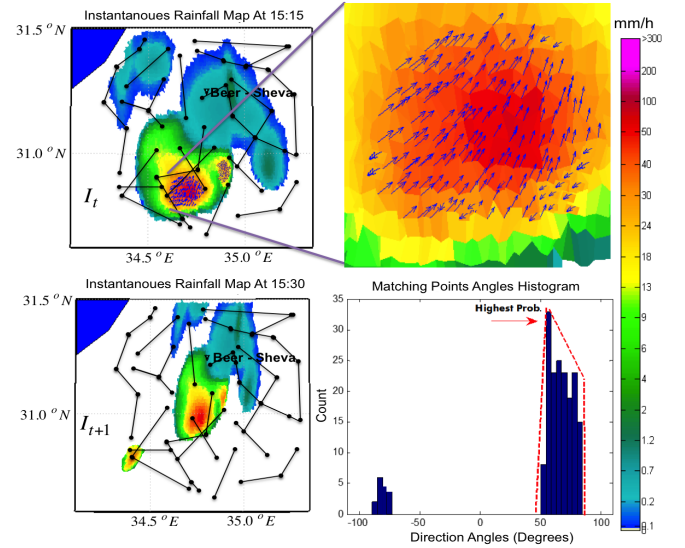

Fig. 2. Example of the proposed algorithm (with only 3 iterations), for finding matching points for two sequential rainfall maps. Top left: the reconstructed rain field from links at 15:15 - I_t. Top right: Zoom in around the highest rain rate intensities observed in I_t, where each direction point is depicted by a blue arrow. Bottom left:the reconstructed rain field from links at 15:30 - I_{t+1}. Bottom right: the direction histogram.

After deriving the space-time model of the rain field (denoted as **H** in (2)) between the inspected sequential rainfall maps, the estimated model was applied on all the coordinates in the area of interest. Next, the dynamically propagated estimates of the rainfall spatial distribution are predicted and corrected while using the Kalman filter, according to the newly observed data, as described in Section 2.1.

2.1. The reconstruction correction

The use of Kalman filter for object tracking is an efficient data assimilation method that explicitly accounts for the dynamic propagation of errors in the model, [9]. For linear models (as was assumed here), the Kalman filter provides an optimal estimate of the state of the system, in terms of minimum estimation error covariance of both the model and observations.

The Kalman filter estimates the spatio-temporal rainfall distribution from a set of non-uniform (possibly sparse) arbitrary network of microwave links. The filter combines past samples with new observations according to the derived relation in (2). Thus, the system of equations, which describes

the state and the measurement equations, are given by:

$$\vec{x}_t = \mathbf{H}\vec{x}_{t-1} + \vec{w}_t \tag{6a}$$

$$\vec{z}_t = \mathbf{M}\vec{x}_t + \vec{q}_t \tag{6b}$$

Where $\vec{x}_t$ indicates the current inspected frame coordinates in the area of interest. $\mathbf{H}$ is the relation matrix between sequential frames (as defined in (2)), $\vec{z}_t$ indicates the current measurement (denoted as the space coordinates in the area of interest), therefore, $\mathbf{M}$ is regarded as the identity matrix.

The noises $\vec{w}_t, \vec{q}_t$ reflect the state noise and the measurement noise, respectively. These noises are regarded as uncorrelated and zero mean noises (i.e., $E\{\vec{q}_t\} = E\{\vec{w}_t\} = \vec{0}$; $E\{\vec{q}_t\vec{w}_t^T\} = \mathbf{0}$). The autocorrelation matrix of $\vec{w}_t$ might be estimated from the state equation defined in (6a), that is: $\mathbf{R} \triangleq E\{\vec{w}_t\vec{w}_t^T\} \approx (\vec{x}_t - \mathbf{H}\vec{x}_{t-1})(\vec{x}_t - \mathbf{H}\vec{x}_{t-1})^T/M$. The autocorrelation matrix of $\vec{q}_t$ (denoted as $\mathbf{Q}$) is defined to be a diagonal matrix with standard deviation of some defined (small enough) threshold, that is, each measurement might have an error of some maximum threshold for each one of the inspected coordinates (e.g., $0.1 \ km$). These noises stand for the inaccuracies that may have occurred in the estimation of the dynamical model when using **Algorithm 1**.

Now, the Kalman equations can be solved. By using a prediction and correction scheme, a dynamical estimate for $\vec{x}_t$, denoted as $\hat{x}_t$, of the rain field can be acquired, given the newly observed, and past, data. The estimates are obtained by minimizing the overall estimation error, which is defined as: $\mathbf{P}_t = E\{(\vec{x}_t - \hat{x}_t)^T(\vec{x}_t - \hat{x}_t)\}$. Thus, the estimation is achieved by iteratively applying the prediction and correction steps, until a solution is reached, as shown in Table. 1:

Table 1. The Kalman filter for object tracking.

Prediction	Correction
$\hat{x}'_{t+1} \approx \mathbf{H}\hat{x}_t$	$\mathbf{K}_t = \mathbf{P}'_t\mathbf{M}^T(\mathbf{M}\mathbf{P}'_t\mathbf{M}^T + \mathbf{R})^{-1}$
$\mathbf{P}'_{t+1} = \mathbf{H}\mathbf{P}_t\mathbf{H}^T + \mathbf{Q}$	$\hat{x}_t = \hat{x}'_t + \mathbf{K}_t(\vec{z}_t - \mathbf{M}\hat{x}'_t)$
	$\mathbf{P}_t = (\mathbf{I} - \mathbf{K}_t\mathbf{M})\mathbf{P}'_t$

Where $\mathbf{K}_t$ is the Kalman gain and $\mathbf{I}$ is the identity matrix.

3. RESULTS AND PERFORMANCE ANALYSIS

In this section the use of the proposed method from Section 2 is demonstrated. The reconstruction of the rainfall map is compared with that of the radar, which is considered as one of the most renowned methods for rainfall mapping today. Moreover, the affect the method has on the achieved performance of the rain field reconstruction is also investigated, when compared to actual rain measures in the inspected area, along with other rainfall mapping techniques, i.e.: the radar, instantaneous mapping and Zinevich et al. method.

Fig. 3 demonstrates the rainfall mapping results when using the proposed method. In the inspected event, links data were observed for 1.5 hours (15:00-16:30), with temporal resolution of 15 minutes, that is, a total of 7 instantaneous rainfall maps. Hence, the proposed novel method was applied on

each sequential frames (e.g., 15:00 and 15:15 frames). In the figure, the reconstructions of the proposed method using ML and the radar are shown. Regarding the radar's images, the $70 \ km$ arc indicates the radius distance from the radar location at Bet-Dagan (32.0^oN, 34.8^oE).
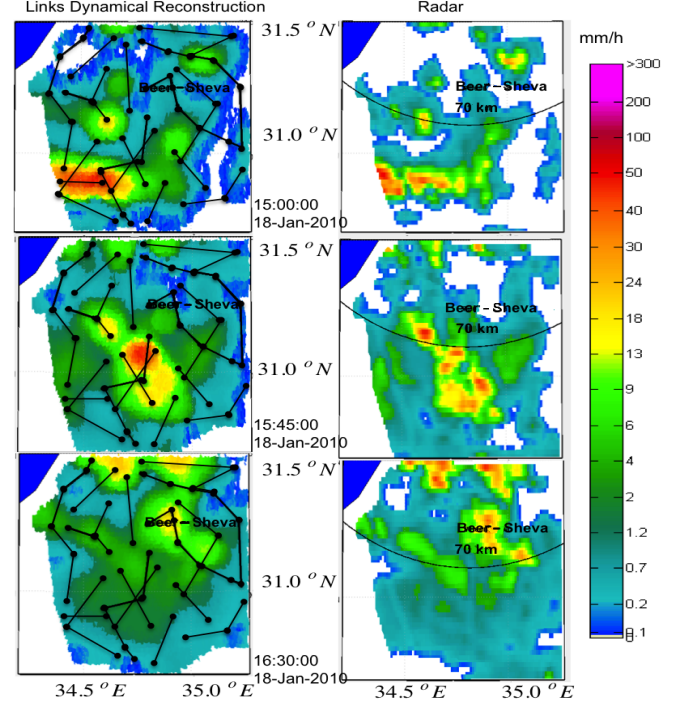

Fig. 3. Recovery of rainfall maps during a rain event. The reconstructions of the proposed method using ML (black lines) and the radar are shown at: 15:00, 15:45 and 16:30 (from top to bottom). Left: The proposed method. Right: The radar.

The inspected region in Fig. 3 consists of a rather sparse ML distribution, comprising of only 36 operating ML in an area of 35X35 km^2. Rain gauges measurements, which are considered as ground truth rain measures, are available in a temporal resolution of 5 minutes, which are provided in 20 different locations within the inspected area. Each rain gauge provides actual rain rate measure in an area of about $1m^2$.

Radar maps are also available in a temporal resolution of 5 minutes. Both the rain gauges and radar maps are provided by the IMS. Thus, due to the different time resolution of each source, only the common times are considered when evaluating the different cost functions:

$$RMSE = (\frac{1}{\tilde{N}\tilde{M}}\sum_{j=1}^{\tilde{M}}\sum_{i=1}^{\tilde{N}}(\hat{x}_{i,j} - x_{i,j})^2)^{\frac{1}{2}} \tag{7a}$$

$$\rho = \frac{\sum_{j=1}^{\tilde{M}}\sum_{i=1}^{\tilde{N}}(\hat{x}_{i,j} - \mu_{\hat{x}})(x_{i,j} - \mu_x)}{(\sum_{j=1}^{\tilde{M}}\sum_{i=1}^{\tilde{N}}(x_{i,j} - \mu_x)^2 \sum_{j=1}^{\tilde{M}}\sum_{i=1}^{\tilde{N}}(\hat{x}_{i,j} - \mu_{\hat{x}})^2)^{\frac{1}{2}}} \tag{7b}$$

$$RE = \frac{1}{\tilde{N}\tilde{M}}\sum_{j=1}^{\tilde{M}}\sum_{i=1}^{\tilde{N}}\frac{|\hat{x}_{i,j} - x_{i,j}|}{x_{i,j}} \tag{7c}$$

Where in (7): ρ is the correlation measure, the $RMSE$ (in

mm/h) is the Root Mean Square Error, and RE is the Relative Error. $\mu_{\hat{x}}$ and μ_x are the mean spatial rain rates of the estimated rain measurements ($\hat{x}_{ij}$) and the true measurements (x_{ij}), respectively. The index j refers to each time step (total of $\tilde{M}$ time steps), while index i refers to the spatial coordinate (total of $\tilde{N}$ inspected coordinates). The performance evaluation of the inspected measures in (7) is detailed in Table. 2.

Table 2. Performance analysis of the instantaneous, proposed method, the advection model and the radar reconstructions.

Method	Correlation	RMSE	RE
Instantaneous	0.721	14.2	60%
Proposed Method	0.873	8.7	34%
Advection	0.645	17.8	65%
Radar	0.752	13.4	55%

4. DISCUSSION

This paper explores the concept of recovering accurate reconstructions of rainfall maps and their dynamics, using microwave links observations and their assimilation into a spatio-temporal model. The performance of the latter has been assessed by comparing the reconstructions of the instantaneous mapping, the radar, the dynamic recovery using the advection model (Section 1) and the proposed method to 20 actual rain measure instruments (rain gauges), in center-south of Israel, in an area of 35X35 km^2.

The instantaneous technique used in this paper for rainfall mapping may yield reconstruction errors, especially in a sparse network, thus providing a quite poor rainfall recovery, as shown in Table. 2. Regarding the proposed reconstruction technique, the method is constrained to a linear model, which is assumed to hold for the space-time model of the rainfall mapping and its dynamics recovery, though this kind of model may not necessarily hold. Hence, more complicated non-linear models, with the use of the extended Kalman filter (EKF), might be considered in the future.

As expected, Zinevich et al. method using the advection model for dynamical reconstruction of rainfall maps showed poor results, with respect to the radar and the proposed method. As explained before, the main reason is that this method requires high temporal resolution of the RSL measurements, along with high spatial resolution of the ML distribution in space, which is not always available in general and in this research in particular.

Regarding the radar's performance, an improvement of about 3% was achieved in the correlation measure, when compared to the instantaneous method. The proposed reconstruction technique not only showed an impressive improvement of more than 15% in all measures, when compared to the instantaneous method, it also outperformed the radar with a 12% improvement in all measures. Moreover, the ability of the method to capture the rainstorm dynamics and to track the rainstorm changes was shown in Fig. 3, where the reconstruction was compared with that of the radar.

Finally, dense CMN at high temporal and spatial resolutions are not available everywhere. It is clear that the quality of the rain field reconstruction, at every point, depends on the availability of nearby links. Nevertheless, even when sparse network is deployed in space, the proposed approach managed to achieve the most accurate reconstruction.

Due to the nature of the problem presented in this paper for accurate recovery of rainfall maps using object tracking extensions, an interesting comparison was also conducted, which compared the proposed method to the well-known optic flow Horn-Schunk method for object tracking, [11]. The latter managed to achieve a correlation of about 82%, which is lower than the one achieved by the proposed method. Thus, proving again the unwavering ability of the technique.

The method proposed here was used for the application of accurate recovery of rainfall maps, though it may also be used for other object tracking or video processing applications.

REFERENCES

[1] H. Messer, A. Zinevich, and P. Alpert, "Environmental monitoring by wireless communication networks," *Science*, vol. 312, no. 5774, pp. 713, 2006.

[2] A.R. Jameson, "A comparison of microwave techniques for measuring rainfall," *Journal of Applied Meteorology*, vol. 30, no. 1, pp. 32–54, 1991.

[3] O. Goldshtein, H. Messer, and A. Zinevich, "Rain rate estimation using measurements from cmn," *IEEE T. Signal Processing*, vol. 57, no. 4, pp. 1616–1625, 2009.

[4] A. Overeem, H. Leijnse, and L.R. Uijlenhoet, "Country wide rainfall maps from cmn," *PNAS*, March 2013.

[5] A. Zinevich, H. Messer, and P. Alpert, "Frontal rainfall observation by cmn," *Journal of Applied Meteorology and Climatology*, vol. 48, no. 7, pp. 1317–1334, 2009.

[6] W. Hundsdorfer and J.G. Verwer, *Numerical solution of time-dependent advection-diffusion-reaction equations*, vol. 33, Springer, 2003.

[7] Y. Liberman, "Optimal recovery of rain field maps using wireless sensors network," M.Sc. Thesis, Tel Aviv University, 2013.

[8] S. Korman and S. Avidan, "Coherency sensitive hashing," in *IEEE International Conference on Computer Vision (ICCV)*. IEEE, 2011, pp. 1607–1614.

[9] G. Bishop and G. Welch, "An introduction to the kalman filter," *Proc of SIGGRAPH, Course*, vol. 8, pp. 27599–3175, 2001.

[10] V. Madhok and D. Landgrebe, "A process model for remote sensing data analysis," *IEEE T.*, vol. 40, no. 3, pp. 680–686, 2002.

[11] Berthold K Horn and Brian G Schunck, "Determining optical flow," in *Technical Symposium East*. Society for Optics and Photonics, 1981, pp. 319–331.